Acetic Anhydride in the Gas Phase, Studied by Electron Diffraction and Infrared Spectroscopy, Supplemented With ab Initio Calculations of Geometries and Force Fields

Guang Wu, C. Van Alsenoy, and H. J. Geise*

Department of Chemistry, University of Antwerpen (UIA), Universiteitsplein 1, B-2610 Wilrijk, Belgium

E. Sluyts and B. J. Van der Veken

Department of Inorganic Chemistry, University of Antwerpen (RUCA), Groenenborgerlaan 171, B-2020 Antwerpen, Belgium

I. F. Shishkov and L.V. Khristenko

Moscow State University, Department of Chemistry, Leninskiye Gori, Moscow 117234, Russia

Received: September 3, 1999; In Final Form: November 30, 1999

Geometry-relaxed ab initio calculations of acetic anhydride at interalia B3LYP/6-31G**, B3LYP/cc-pvtz, and MP2/6-31G** level revealed a mixture of nonplanar (sp,sp) and (sp,ac) energy minima, connected to one another via low-energy rotation barriers, thereby allowing for extensive large-amplitude motions. This model provided the geometrical constraints and force fields necessary to perform the joint analysis of gas-phase electron diffraction and infrared data. The large-amplitude motion is described, using pseudoconformers at 20° intervals around the axes of rotation. It led to a dynamic model consisting of eight pseudoconformers of lowest energy connected to the two local minima ((sp,ac) and nonplanar (sp,sp)) by fixed differences in torsion angles. The main structural parameters were refined using the electron diffraction method and an experimental "conformer" ratio of nonplanar (sp,sp)/(sp,ac) = 37(±15)%:63(±15)% was obtained, in close agreement with the quantum chemical results. The model of acetic anhydride is self-consistent, reproduces the IR frequencies, with a root-mean-square deviation of about 10 cm^{-1}, and results in an improved frequency assignment. Assisted by MP2/6-31G**-based IR band intensities, the model also explains the following experimental spectral peculiarities: (i) the relatively large number of bands with a small intensity and (ii) the changes in band intensities, band shape, and doublet behavior when going from the gas phase to the liquid and to solutions of different polarity.

Introduction

In our ongoing research program into the conformational analysis and vibrational spectroscopy of molecules governed by two rotors, we investigated acetic anhydride (henceforth abbreviated as AA), $H_3C(O)OC(O)CH_3$. The torsion angles ϕ_1 (O(9)═C(8)−O(1)−C(2)) and ϕ_2 (O(3)═C(2)−O(1)−C(8)) characterize the various possible conformations of the heavy-atom skeleton. Planar and nonplanar rotamers are shown in Figure 1, together with their IUPAC names[1] and the atomic numbering scheme used.

AA is a widely used reagent in organic synthesis, but surprisingly, little reliable information is available about its conformational space and spectroscopy. Therefore, it is of some interest to compare AA with formic anhydride (FA) and formic acetic anhydride (FAA), which we studied before and found to have planar (sp,ap) conformations.[2,3] As far as we know, microwave studies of AA are missing, and studies on vibrational spectroscopy,[4,5] electron diffraction,[6] and ab initio calculations[7] have been mainly performed in a stand-alone fashion. The results seemed to favor the occurrence in the gas phase of a nonplanar form with C_2 symmetry, possibly an (sp,sp) form.

However, there is a discrepancy between the interpretations of the infrared and electron diffraction investigations. The 4-31G calculations of Colthup[7] in conjunction with the experimental value of Mirone et al.[4] for the integrated intensity ratio A_a/A_s of the antisymmetric and symmetric carbonyl stretch bands led to the estimate $\phi_1 = \phi_2 = 33°$, whereas the electron diffraction experiments of Vledder et al.[6] resulted in the significantly higher value $\phi_1 = \phi_2 = 49(1)°$.

Furthermore, the presence of many weak bands and shoulders, as well as the almost complete lack of PQR separations make the IR spectrum complex. Therefore, it is not surprising that disagreement also exists between two IR assignments.[4,5] Moreover, Mirone et al.[4] concluded on the occurrence of one nonplanar conformation with C_2 symmetry, i.e., an (sp,sp) or an (sc,sc) form. The authors excluded the occurrence of more than one conformer and ascribed the band shape in the C═O region as well as most of the shoulders in other regions to Fermi resonance. In contrast, Vledder et al.[5] interpreted the peculiarities of the spectra in terms of the high flexibility of the AA molecule. Mindful of the electron diffraction observations, they stressed the importance of large-amplitude motions. Thus, they allowed for an extended distribution of torsion angles, but did not specify the symmetry of the other forms they implicitly considered as possible.

Neither of these researchers was able to rationalize the behavior of the IR doublet at 800 cm^{-1} and the other spectral

* To whom correspondence should be addressed.

10.1021/jp993131z CCC: $19.00
Published on Web 01/29/2000

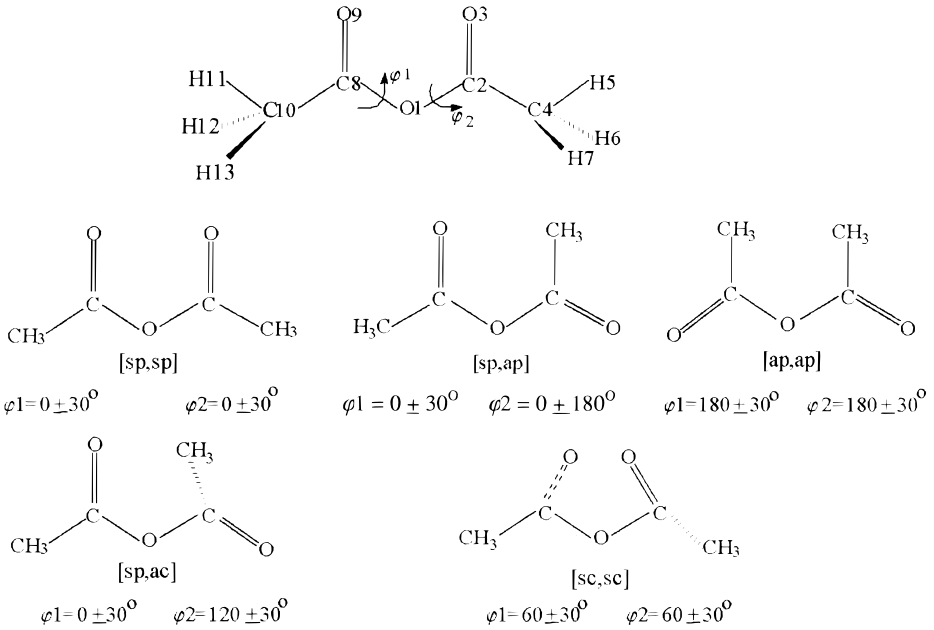

Figure 1. Some planar and nonplanar conformations of AA, together with definitions of torsion angles and the atomic numbering scheme used.

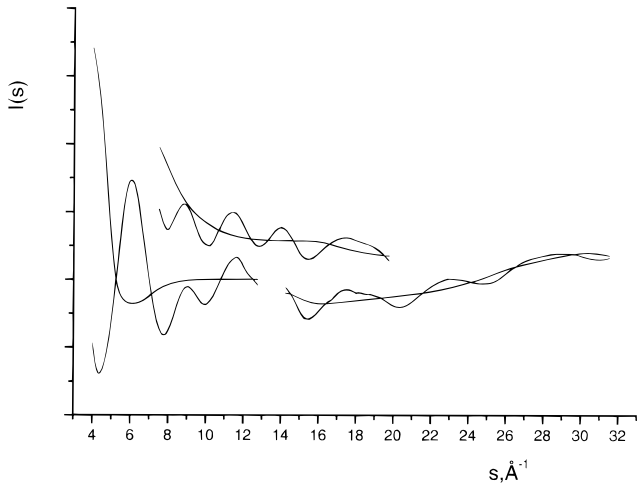

Figure 2. Experimental leveled intensities $I(s)$ with final backgrounds, $B(s)$, for AA.

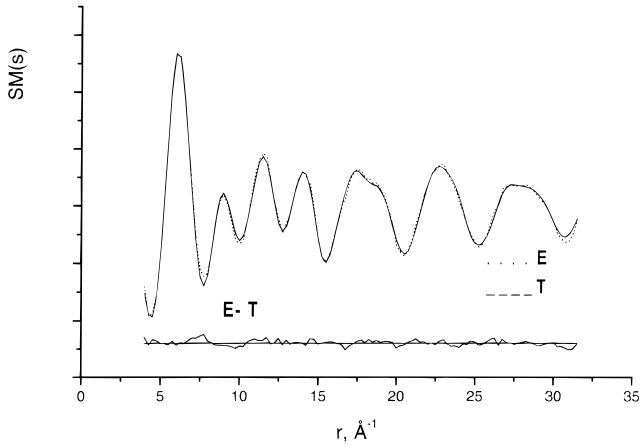

Figure 3. Experimental (○) and theoretical (—) $sM(s)$ curve for AA.

changes that occur when AA goes from the gaseous to the liquid state and to solutions.

The purpose of this study is to produce, with the help of ab initio calculations, (i) a self-consistent molecular model that simultaneously rationalizes infrared and electron diffraction data in the gas phase, (ii) complete harmonic force fields to distinguish between some of the conflicting interpretations of the IR data, and (iii) a model capable of rationalizing the phase dependency of the IR spectra.

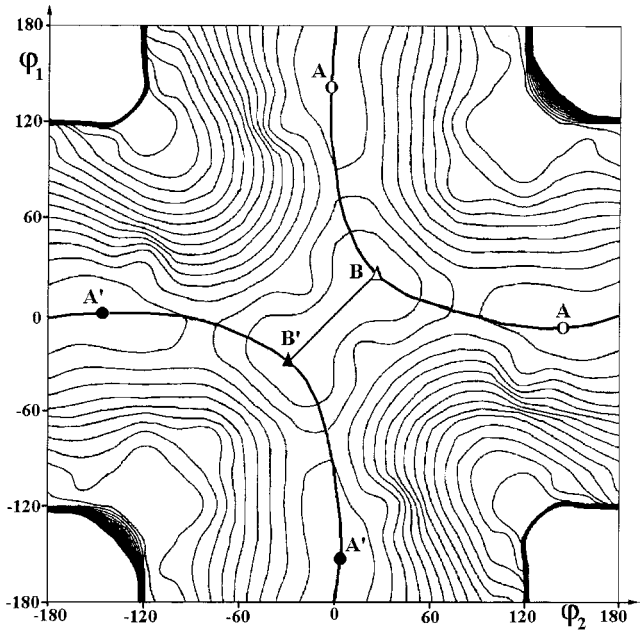

Figure 4. Conformational energy map of AA as a function of ϕ_1 and ϕ_2, resulting from 4-21G calculations. Equipotential contours are drawn at intervals of 1 kcal/mol. Energy minima are shown on the rotation pathways (AB′A; A′BA; BB′). (sp,ac) rotamers at $\phi_1 = -a$, $\phi_2 = +b$ and at $\phi_1 = +b$, $\phi_2 = -a$ are denoted by (○), their mirror images at $\phi_1 = +a$, $\phi_2 = -b$ and $\phi_1 = -b$, $\phi_2 = +a$ by (●), and the nonplanar (sp,sp) rotamers at $\phi_1 = \phi_2 = +c$ and $\phi_1 = \phi_2 = -c$ by (Δ) and (▲), respectively.

Experimental Section

A commercial sample of acetic anhydride (MERCK, analytical grade) was treated with P_2O_5, followed by Na_2CO_3, and then distilled.

Electron diffraction data were recorded photographically on the Antwerpen diffraction unit manufactured by Technisch

TABLE 1: Relative Energies (kcal/mol) and Positions (φ_1 , φ_2; Degrees) of Energy Minimum and Maximum Forms along the Lines ABA and BB′ (see Figure 4), Calculated at Various Levels of Sophistication

	energy minima				energy maxima, barrier heights		
	[sp,sp]; C_2		[sp,ac]; C_1		[sp,sc]; C_2	[sp,ap]; C_s	[sp,sp]; C_{2v}
	rel E	φ_1, φ_2	rel E	φ_1, φ_2	rel E $\varphi_1 = 0$ $\varphi_2 = 60$	rel E $\varphi_1 = 0$ $\varphi_2 = 180$	rel E $\varphi_1 = 0$ $\varphi_2 = 0$
HF/4-21G	0	22; 22	1.04	−3; 137	2.51	1.29	0.26
HF/6-31G**	0	31; 31	0.20	−2; 108	1.05	0.91	1.02
MP2/6-31G**	0	27; 27	0.30	−2; 113	0.91	0.73	0.76
B3LYP/6-31G**	0.05	28; 28	0	−8; 152	1.27	0.17	0.78
B3LYP/CC-PVTZ	0	30; 30	0.13	−9; 149	1.14	0.42	1.15

Physische Dienst, TPD-TNO, Delft, The Netherlands. A description is given in ref 8. Because of the relatively low volatility of AA, the experiments were performed at a nozzle temperature of 70 °C and a sample temperature of 60 °C.

An accelerating voltage of 60 kV, stabilized within 0.01% during the exposures, was employed. The electron wavelength was calibrated against the known CC bond length of benzene,[9] resulting in $\lambda = 0.048712(2)$ Å. Three, three, and four plates (Kodak Electron Image) were selected from recordings at the nozzle-to-plate distances of 199.41(2), 350.98(2), and 600.05(2) mm, respectively. Optical densities were measured on a modified, microprocessor-controlled rotation ELSCAN E-2500 microdensitometer.[10] Optical density values were converted to intensities using the one-hit model of Forster.[11] Coherent scattering factors were taken from Ross et al.,[12] and incoherent scattering factors from Tavard et al.[13] The data were further processed by standard procedures,[14] yielding leveled intensities in the following ranges:

$$60 \text{ cm}: 4.00 \le s \le 12.75 \text{ Å}^{-1}$$

$$35 \text{ cm}: 7.50 \le s \le 19.75 \text{ Å}^{-1}$$

$$20 \text{ cm}: 14.00 \le s \le 31.75 \text{ Å}^{-1}; \quad \text{all with } \Delta s = 0.25 \text{ Å}^{-1}$$

Leveled intensities with final backgrounds and the combined $sM(s)$ curve are shown in Figures 2 and 3, respectively. Details about the processing of electron diffraction data may be found in refs 15 and 16.

Gas-phase infrared spectra between 4000 and 50 cm^{-1} were recorded at room temperature at a pressure of 5 hPa on a Bruker 113V FTIR spectrophotometer. A broadband MCT detector was used in the range 4000−600 cm^{-1}, a DTGS detector in the range 600−300 cm^{-1}, and a liquid helium cooled silicon bolometer in the 350−50 cm^{-1} range. The spectra of 0.2 M solutions in CCl_4 and other solvents, of the liquid phase as well as of the solid state were measured on the same instrument.

The comparison with the frequencies observed by Vledder et al.[5] for the d_o species shows a root-mean-square deviation of 11.1 cm^{-1} and a maximum deviation of 26 cm^{-1}. The comparison with the frequencies by Mirone et al.[4] gives a rms deviation of 7.5 cm^{-1} and a maximum deviation of 18 cm^{-1}. A rms of 13.5 cm^{-1} and a maximum deviation of 31 cm^{-1} was found between the data of Vledder and Mirone. These large differences give clear evidence of the difficulties in distinguishing the weak fundamentals from other vibrations and even from noise. Moreover, the broad, often weak bands will suffer from a low resolution.

Theoretical Models

Apart from a not-relaxed study,[7] no ab initio calculations on AA have been published. In this work, ab initio calculations were performed using Pulay's gradient method,[17−19] the program BRABO,[20] and the program Gaussian 98.[21] In the first stage, we calculated on the 4-21 G level the complete conformational energy map of AA as a function of the torsion angles ϕ_1 and ϕ_2 in steps of 20°, while optimizing the other geometrical parameters. Figure 4 depicts the results, from which the following emerges. First, none of the planar forms (Figure 1) is a minimum energy form. Energy minima are only found (Table 1) for a nonplanar (sp,sp) form near $\phi_1 = \phi_2 = +22°$ (called B in Figure 4) and a nonplanar (sp,ac) form near $\phi_1 = -3°$ and $\phi_2 = +137°$ (called A in Figure 4). In AA, a form at $\phi_1 = -a$, and $\phi_2 = +b$ and one at $\phi_1 = +b$, $\phi_2 = -a$ are identical. Obviously, their energy and distance distribution are equal to those of their mirror images (called B′ and A′ in Figure 4). Thus, in the interval $-180° \le \phi_1, \phi_2 \le +180°$ there are six minima, linked in pairs through an inversion center at $\phi_1 = \phi_2 = 0°$. Second, these minima are located in a system of low-energy valleys, strongly suggesting that the molecule exhibits large-amplitude motions, interconnecting the pseudorotamers (A, A′, B, B′). Third, one section of the rotational pathways connects A → B (and B′ → A′) with a barrier form (energy maximum) approximately halfway between A and B, i.e., located at $\phi_1 = 0$ and $\phi_2 = 0.5$ (ϕ_1 (A) + ϕ_2 (B)), (and equivalent points). The validity of the latter was confirmed by energy calculations scanning ϕ_1 in steps of 10° in the range 50°−100°. The other two sections of the pathways connect B → B′ with the barrier form (energy maximum) located at $\phi_1 = \phi_2 = 0°$ and A → A′ with the barrier form at $\phi_1 = 0$, $\phi_2 = 180°$ (and equivalent points).

To define more accurately the position, geometry, and energy of these pseudorotamers of minimum and maximum energy, we explored their ϕ_1, ϕ_2 environs at the 6-31G**, the MP2/6-31G**, the B3LYP/6-31G**, and the B3LYP/cc-pvtz level. From the results, also given in Table 1, one notes that except B3LYP/6-31G** all approaches calculate the nonplanar (sp,sp) form to be more stable than the (sp,ac) form. All approaches, however, agree that the differences between the energy minima are small and that the barrier heights between them are low. Hence, we conclude that gaseous AA performs complicated large-amplitude motions involving all atoms. Moreover, an analysis of permutation-inversion groups[22] shows that the ensemble of molecular forms in dynamic equilibrium over its entire rotation space behaves as a molecule with C_2 symmetry, even though some individual forms have C_1 symmetry. This already demonstrates that C_2 symmetry as suggested by IR spectroscopy and the occurrence of more than one conformation are not mutually exclusive.

The geometry of the minimum and maximum energy forms met along the ϕ_1, ϕ_2 rotations pathways, calculated at the MP2/6-31G** and the B3LYP/cc-pvtz level are collected in Table 2. They reveal a number of conformational dependencies in bond lengths and valence angles, some of which can be rationalized by the mesomeric interaction in the $COC(O)CH_3$ fragments and

TABLE 2: Optimized Geometries (r_e-Type, Distances in Å, Angles in Degrees) of Energy Minimum and Maximum Forms[a] along the Lines ABA and BB′ (see Figure 4), Calculated at Various Levels of Sophistication

	energy minima				energy maxima		
	[sp,sp]; C_2		[sp,ac]; C_1		[sp,sc]; C_2	[sp,ap]; C_S	[sp,sp] C_{2v}
parameters	MP2 6-31G**	B3LYP CC−PVTZ	MP2 6-31G**	B3LYP CC-PVTZ	B3LYP CC-PVTZ	B3LYP CC-PVTZ	B3LYP CC-PVTZ
C(2)−O(1)	1.400	1.395	1.430	1.408	1.411	1.406	1.397
C(8)−O(1)	1.400	1.395	1.369	1.374	1.383	1.378	1.397
C(2)═O(3)	1.200	1.191	1.195	1.191	1.188	1.192	1.189
C(8)═O(9)	1.200	1.191	1.210	1.198	1.194	1.197	1.189
C(2)−C(4)	1.501	1.500	1.497	1.499	1.498	1.499	1.504
C(8)−C(10)	1.501	1.500	1.501	1.502	1.502	1.502	1.504
C(2)−O(1)−C(8)	118.56	120.98	115.85	124.42	119.89	127.26	124.12
O(1)−C(2)═O(3)	123.70	123.04	118.79	116.75	121.95	115.58	125.21
O(1)−C(2)−C(4)	108.98	109.97	113.18	117.48	110.65	119.42	108.38
C(4)−C(2)═O(3)	127.17	126.94	127.73	125.64	127.32	125.01	126.41
O(1)−C(8)═O(9)	123.70	123.04	123.45	124.25	123.66	125.22	125.21
O(1)−C(8)−C(10)	108.98	109.97	110.07	109.73	109.72	109.02	108.38
C(10)−C(8)═O(9)	127.17	126.94	126.46	125.99	126.63	125.76	126.41
O(9)═C(8)−O(1)−C(2)	26.94	30.37	−2.26	−8.82	0	0	0
O(3)═C(2)−O(1)−C(8)	26.94	30.37	113.18	148.88	60	180	0
dipole (D)	4.54	3.83	3.71	2.53	3.98	1.94	4.37
			Inertia Moments				
A (GHz)	5.4509	5.5011	5.1887	5.3094	5.3313	5.3195	5.4908
B (GHz)	1.8224	1.7826	1.8226	1.8691	1.8045	1.9084	1.8566
C (GHz)	1.5172	1.5290	1.6582	1.4985	1.5562	1.4290	1.4116

[a] For brevity sake, geometries are listed of the heavy-atom skeleton only. The C−CH_3 moieties have a quasiperfect tetrahedral arrangement.

the steric hindrance between them. Obviously, the mesomeric effect is largest when the fragment is in the planar sp or ap position, and causes the C−O bond order to increase and that of C═O to decrease. Hence, one expects upon rotation of the acetyl fragment the C−O lengths in the order sp < ap < sc ≈ ac and C═O lengths in the order sp > ap > sc ≈ ac.

The mesomeric effect on valence angles is to decrease the O═C−O(1) and to increase the CH_3−C−O(1) angles, because of the growing importance of the charged resonance hybrid O^-−C═O^+(1), while the rocking movement of the acetyl group keeps the O═C−CH_3 angle quasiconstant. These variations show (Table 2) indeed in the angles of the O(3)═C(2)(C(4))−O(1) moiety going from the nonplanar (sp,sp) → (sp,sc) → (sp,ac) → (sp,ap) form.

The variations seen in the angles of the O(9)═C(8)(C(10))−O(1) moiety in the same rotameric sequence reflect the response of the moiety in sp position to rotation of the *other* COC(O)-CH_3-group. These small variations cannot be dominated by the mesomeric effect because the position of the O(9)═C(8)-(C(10))−O(1) moiety is sp in all cases. The dominant effect here is the steric hindrance the two acetyl halves exercise on each other. Its influence is large in the planar and less in the nonplanar forms and tends to increase the C(2)−O(1)−C(8) and O(1)−C(8)═O(9) angles and to decrease the C(10)−C(8)−O(1) angle, with which the observed variations are in agreement.

Vibrational Spectroscopy

Using the MP2/6-31G** basis set, we calculated the harmonic force fields of the nonplanar (sp,sp) and (sp,ac) rotamers of AA by applying Gaussian 98. The force constant matrices, obtained in Cartesian coordinates, were transformed to the local symmetry coordinates (Table 3) and used to calculate vibrational frequencies and band intensities. With the help of the latter intensities, the experimental IR frequencies could be assigned with the unscaled force fields. To obtain a better agreement between theoretical and experimental frequencies the force fields were scaled by the program SCAL,[23] designed for interactive refinement of quantum mechanical molecular force fields by least squares.[24] The scaling method is that of Pulay et al.[25] The number of quasiequivalent internal coordinates (e.g., all stretching C−H or deformation C−H vibrations can be considered as quasiequivalent) fixes the maximum number of scale factors to 10. On the other hand the number of scale factors and the way the symmetry coordinates are distributed over the scale factor groups should reflect the fact that the scale factors are called into existence to counteract the systematic errors in the computations. One may expect the errors in stretching constants to be different from those in, e.g., torsion constants, and those in C−H stretchings to be different from those in non-CH stretchings. This reasoning helps to select the grouping of the symmetry coordinates in a systematical way. We tried eight such groupings, the largest with 10, the smallest with five scale factors. To discriminate among the eight runs one may compare the ratio of the *R* values ($R = \{\sum_i[v_i(\text{obs}) - v_i(\text{calc})]^2/\sum v_i(\text{obs})^2\}^{1/2}$ of two such groupings with tabulated[26] values of $P(p,n-p,\alpha)$, in which *p* denotes the degrees of freedom (here number of scale factors), *n* the number of data points (here number of frequencies), and α the chosen level of significance. If the ratio is larger than *P*, then one rejects the hypothesis that the two runs are equal in performance at the 100α% significance level. Executing the test at the 5% level of significance the run with five scale factors performed statistically as well as the one with 10 scale factors, and hence the former is preferred (Table 4). The fit between experimental and scaled calculated frequencies is good with physically realistic root-mean-square (rms) and maximum deviations (Δ max) that are close to rms and Δ max values found between experimental frequency sets (see Experimental Section). The scaling results (Table 5) clearly indicate that the force fields perform very well in reproducing the experimental frequencies. Hence, the following spectral analysis is focused on them. Here, we also mention that the absolute band intensities, also presented in Table 5, are an invaluable aid in the frequency assignment discussed below as well as in checking the validity of the self-consistent molecular model used in the electron diffraction analysis (see next section).

TABLE 3: Definitions of Symmetry Coordinates S_i in Terms of Internal Coordinates

nonplanar (sp,sp) conformer		(sp,ac) conformer	
specification	symmetry species and assignment	specification	assignment
$S1 = r(1,2) + r(1,8)$	A, r_s C−O	$S1 = r(1,2)$	r, C(2)−O(1)
$S2 = r(2,3) + r(8,9)$	A, r_s C═O	$S2 = r(2,3)$	r, C(2)═O(3)
$S3 = r(2,4) + r(8,10)$	A, r_s C−C	$S3 = r(2,4)$	r, C(2)−C(4)
$S4 = [r(4,5) + r(4,6) + r(4,7)] + [r(10,11) + r(10,12) + r(10,13)]$	A, r_s C−H	$S4 = r(4,5) + r(4,6) + r(4,7)$	r_s, C(4)−H
$S5 = [2r(4,5) - r(4,6) - r(4,7)] + [2r(10,11) - r(10,12) - r(10,13)]$	A, r_{as} C−H	$S5 = 2r(4,5) - r(4,6) - r(4,7)$	r_{as}, C(4)−H
$S6 = [r(4,6) - r(4,7)] + [r(10,12) - r(10,13)]$	A, r_{as} C−H	$S6 = r(4,6) - r(4,7)$	r_{as}, C(4)−H
$S7 = [\theta(5,4,6) + \theta(5,4,7) + \theta(6,4,7) - \theta(2,4,5) - \theta(2,4,6) - \theta(2,4,7)] + [\theta(11,10,12) + \theta(11,10,13) + \theta(12,10,13) - \theta(8,10,11) - \theta(8,10,12) - \theta(8,10,13)]$	A, δ_s C−H bending	$S7 = \theta(5,4,6) + \theta(5,4,7) + \theta(6,4,7) - \theta(2,4,5) - \theta(2,4,6) - \theta(2,4,7)$	δ_s, C(4)−H bending
$S8 = [2\theta(6,4,7) - \theta(5,4,6) - \theta(5,4,7)] + [2\theta(12,13,10) - \theta(11,10,12) - \theta(11,10,13)]$	A, δ_{as} C−H bending	$S8 = 2\theta(6,4,7) - \theta(5,4,6) - \theta(5,4,7)$	δ_{as}, C(4)−H bending
$S9 = [\theta(5,4,6) - \theta(5,4,7)] + [\theta(13,10,11) - \theta(12,10,11)]$	A, δ_{as} C−H bending	$S9 = \theta(5,4,6) - \theta(5,4,7)$	δ_{as}, C(4)−H bending
$S10 = [2\theta(2,4,5) - \theta(2,4,6) - \theta(2,4,7)] + [2\theta(8,10,11) - \theta(8,10,12) - \theta(8,10,13)]$	A, ρ C−H bending	$S10 = 2\theta(2,4,5) - \theta(2,4,6) - \theta(2,4,7)$	ρ, C(4)−H bending
$S11 = [\theta(2,4,6) - \theta(2,4,7)] + [\theta(8,10,12) - \theta(8,10,13)]$	A, ρ C−H bending	$S11 = \theta(2,4,6) - \theta(2,4,7)$	ρ, C(4)−H bending
$S12 = [2\theta(1,2,3) - \theta(3,2,4) - \theta(1,2,4)] + [2\theta(1,8,9) - \theta(9,8,10) - \theta(1,8,10)]$	A, δ O═C−C bending	$S12 = 2\theta(1,2,3) - \theta(3,2,4) - \theta(1,2,4)$	δ, O(3)═C(2)−O(1) bending
$S13 = [\theta(3,2,4) - \theta(1,2,4)] + [\theta(9,8,10) - \theta(1,8,10)]$	A, ρ_r O═C−C bending	$S13 = \theta(3,2,4) - \theta(1,2,4)$	ρ_r, O(3)═C(2)−C(4) bending
$S14 = \chi(3,1,4,2) + \chi(9,1,10,8)$	A, π O═C−C out-of-plane bending	$S14 = \chi(3,1,4,2)$	π, O(3)═C(2)−C(4) out-of-plane bending
$S15 = [\iota(1,2,4,5) + \iota(3,2,4,5) + \iota(1,2,4,6) + \iota(3,2,4,6) + \iota(1,2,4,7) + \iota(3,2,4,7)] + [\iota(1,8,10,11) + \iota(9,8,10,11) + \iota(1,8,10,12) + \iota(9,8,10,12) + \iota(1,8,10,13) + \iota(9,8,10,13)]$	A, ι C−C torsion	$S15 = \iota(1,2,4,5) + \iota(3,2,4,5) + \iota(1,2,4,6) + \iota(3,2,4,6) + \iota(1,2,4,7) + \iota(3,2,4,7)$	ι, C(4)−C torsion
$S16 = [\iota(8,1,2,3) + \iota(8,1,2,4)] + [\iota(2,1,8,9) + \iota(2,1,8,10)]$	A, ι C−O torsion	$S16 = \iota(8,1,2,3) + \iota(8,1,2,4)$	ι, C(2)−O(1) torsion
$S17 = \theta(2,1,8)$	A, δ C(2)−O(1)-C(8) bending	$S17 = \theta(2,1,8)$	δ, C(2)−O(1)-C(8) bending
$S18 = r(1,2) - r(1,8)$	A, r_{as} C−O	$S18 = r(1,8)$	r, C(8)−O(1)
$S19 = r(2,3) - r(8,9)$	B, r_{as} C═O	$S19 = r(8,9)$	r, C(8)═O(9)
$S20 = r(2,4) - r(8,10)$	B, r_{as} C−C	$S20 = r(8,10)$	r, C(8)−C(10)
$S21 = [r(4,5) + r(4,6) + r(4,7)] - [r(10,11) + r(10,12) + r(10,13)]$	B, r_s C−H	$S21 = r(10,11) + r(10,12) + r(10,13)$	r_s, C(10)−H
$S22 = [2r(4,5) - r(4,6) - r(4,7)] - [2r(10,11) - r(10,12) - r(10,13)]$	B, r_{as} C−H	$S22 = 2r(10,11) - r(10,12) - r(10,13)$	r_{as}, C(10)−H
$S23 = [r(4,6) - r(4,7)] - [r(10,12) - r(10,13)]$	B, r_{as} C−H	$S23 = r(10,12) - r(10,13)$	r_{as}, C(10)−H
$S24 = [\theta(5,4,6) + \theta(5,4,7) + \theta(6,4,7) - \theta(2,4,5) - \theta(2,4,6) - \theta(2,4,7)] - [\theta(11,10,12) + \theta(11,10,13) + \theta(12,10,13) - \theta(8,10,11) - \theta(8,10,12) - \theta(8,10,13)]$	B, δ_s C−H bending	$S24 = \theta(11,10,12) + \theta(11,10,13) + \theta(12,10,13) - \theta(8,10,11) - \theta(8,10,12) - \theta(8,10,13)$	δ_s, C(10)−H bending
$S25 = [2\theta(6,4,7) - \theta(5,4,6) - \theta(5,4,7)] - [2\theta(12,13,10) - \theta(11,10,12) - \theta(11,10,13)]$	B, δ_{as} C−H bending	$S25 = 2\theta(12,13,10) - \theta(11,10,12) - \theta(11,10,13)$	δ_{as}, C(10)−H bending
$S26 = [\theta(5,4,6) - \theta(5,4,7)] - [\theta(13,10,11) - \theta(12,10,11)]$	B, δ_{as} C−H bending	$S26 = \theta(13,10,11) - \theta(12,10,11)$	δ_{as}, C(10)−H bending
$S27 = [2\theta(2,4,5) - \theta(2,4,6) - \theta(2,4,7)] - [2\theta(8,10,11) - \theta(8,10,12) - \theta(8,10,13)]$	B, ρ C−H bending	$S27 = 2\theta(8,10,11) - \theta(8,10,12) - \theta(8,10,13)$	ρ, C(10)−H bending
$S28 = [\theta(2,4,6) - \theta(2,4,7)] - [\theta(8,10,12) - \theta(8,10,13)]$	B, ρ C−H bending	$S28 = \theta(8,10,12) - \theta(8,10,13)$	ρ, C(10)−H bending
$S29 = [2\theta(1,2,3) - \theta(3,2,4) - \theta(1,2,4)] - [2\theta(1,8,9) - \theta(9,8,10) - \theta(1,8,10)]$	B, δ O═C−C bending	$S29 = 2\theta(1,8,9) - \theta(9,8,10) - \theta(1,8,10)$	δ, O(9)═C(8)−O(1) bending
$S30 = [\theta(3,2,4) - \theta(1,2,4)] - [\theta(9,8,10) - \theta(1,8,10)]$	B, ρ_r O═C−C bending	$S30 = \theta(9,8,10) - \theta(1,8,10)$	ρ_r, O(9)═C(8)−C(10) bending
$S31 = \chi(3,1,4,2) - \chi(9,1,10,8)$	B, π O═C−C out-of-plane bending	$S31 = \chi(9,1,10,8)$	π, O(9)═C(8)−C(10) out-of-plane bending
$S32 = [\iota(1,2,4,5) + \iota(3,2,4,5) + \iota(1,2,4,6) + \iota(3,2,4,6) + \iota(1,2,4,7) + \iota(3,2,4,7)] - [\iota(1,8,10,11) + \iota(9,8,10,11) + \iota(1,8,10,12) + \iota(9,8,10,12) + \iota(1,8,10,13) + \iota(9,8,10,13)]$	B, ι C−C	$S32 = \iota(1,8,10,11) + \iota(9,8,10,11) + \iota(1,8,10,12) + \iota(9,8,10,12) + \iota(1,8,10,13) + \iota(9,8,10,13)$	ι, C(10)−C torsion
$S33 = [\iota(8,1,2,3) + \iota(8,1,2,4)] - [\iota(2,1,8,9) + \iota(2,1,8,10)]$	B, ι C−O	$S33 = \iota(2,1,8,9) + \iota(2,1,8,10)$	ι, C(8)−O(1) torsion

3500−2000 cm^{-1}. In this region, one observes only three weak bands due to the CH stretchings. The calculations indicate that the 12 CH stretching modes occur in three clusters, each containing four vibrations of a particular combination of symmetry coordinates, two of which are due to isolated methyl vibrations ((sp,ac) form) and two to coupled methyl vibrations

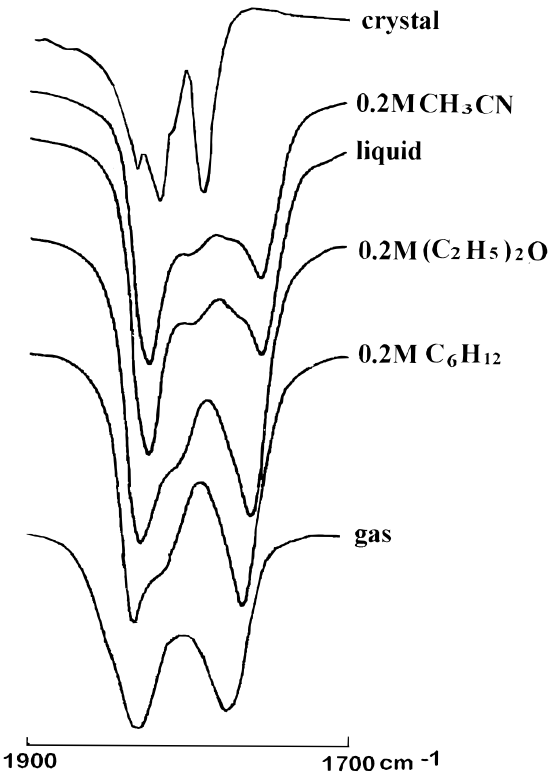

Figure 5. The C═O stretching range in the infrared spectra of AA, obtained in various phases with decreasing dielectric constant from top to bottom ($\epsilon(CH_3CN) = 37.5$; ϵ(liquid AA) = 22; ϵ(ether) = 4.3; $\epsilon(C_6H_{12}) = 2.0$).

(A,B type; nonplanar (sp,sp) form). We assigned the sequence as υ_{as} (at 3040 cm^{-1}), υ_{as} (at 3005 cm^{-1}), υ_{sym} (at 2952 cm^{-1}), different from ref 5 and more detailed than in ref 4. The choice is supported by the agreement between the observed and the calculated intensity sequence.

2000−1600 cm^{-1}. This region exhibits two carbonyl stretches (υ_4 at 1835 cm^{-1} and υ_5 at 1779 cm^{-1}), a phenomenon well-known in anhydrides. The splitting between the symmetric and antisymmetric C═O stretching was attributed by Vledder[5] to the existence of large positive f(C═O, C−O) interaction force constants. Our computations corroborate this. Both bands have a rounded-off shape and lack any sign of rotational structure, a behavior in agreement with the existence of multiple conformations and large-amplitude motion. As with the CH stretching vibrations, the agreement between the four calculated C═O stretching frequencies (two for each rotamer) and the two observed frequencies is excellent.

TABLE 4: Definition of Groups of Vibrations Used in the Scaling of the Force Fields, Together with the Results of the Scaling Procedure

group	vibration	scale factor
1	all C−H stretchings	0.913
2	all other stretchings	0.962
3	all C−H deformations	0.933
4	all other deformations	0.982
5	torsions, τ(CC) and τ(CO)	0.868

Performance[a]

	nonplanar sp,sp	sp,ac
rms (cm^{-1})	13.8	12.3
max. deviation (cm^{-1})	29	31

[a] Measured as the root-square and maximum deviation between the experimental frequency set and the frequencies calculated after the scaling procedure (Table 5).

The intensity ratio of the C═O bands in anhydrides has been correlated[27,28] to the angle (α) between the C═O dipoles via

$$A_{asym}/A_{sym} = tg^2(\alpha/2) \quad (1)$$

Equation 1 was later used[4,7] to obtain information about the torsion angles ϕ_1 and ϕ_2 and about the conformation(s) of AA. It led to a form of C_2 symmetry with $30° \leq \phi_1 = \phi_2 \leq 85°$ (an (sc,sc) form in the IUPAC nomenclature) as the dominant species in the gas phase. However, Vledder et al.[5] stated that the considerable contributions of symmetry coordinates other than S_2 and S_{19} (Table 3) in υ_4 and υ_5 make it impossible to draw conclusions about the AA conformation from eq 1. About the same time, Mirone et al.[4] questioned even the basic assumptions made in the derivation of eq 1. That is to say that the factors determining the A_{asym}/A_{sym} ratio in AA remained hitherto unknown.

Our explanation reads as follows. The rotamers exhibit large-amplitude motions and are in equilibrium with each other. On the time scale of molecular vibrations (IR spectroscopy), the equilibrium is dynamic. Electron diffraction analysis (see below) in the dynamic approximation has shown that the experimental conformer ratio (sp,sp)/(sp,ac) is 37(±15)%:63(±15%). This

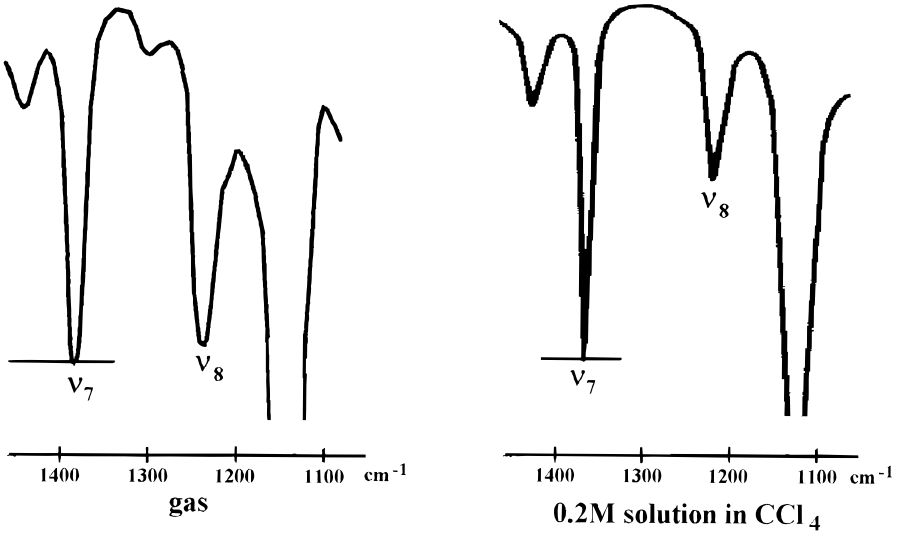

Figure 6. Phase dependency of the band υ_8 in comparison to υ_7.

TABLE 5: Comparison between MP2/6-31G Calculated and Experimental IR Frequencies (cm^{-1}),[a] Together with Calculated Band Intensities (A) and Potential Energy Distributions[b] and Assignments of Modes to the Nonplanar (sp,sp) and (sp,ac) Forms**

conformer		nonplanar (sp,sp)				(sp,ac)			
ν	$freq_{obsd}$	$freq_{calcd}$	A_{calcd}	potential distribution (%)	assignment	$freq_{calcd}$	A_{calcd}	potential distribution(%)	assignment
ν_1	3040 vw	3048	0.010	S5(98)	A ν_{AS} C−H	3050	0.230	S22(98)	ν_{as} C(10)−H
	3040 vw	3048	0.075	S22(98)	B ν_{AS} C−H	3047	0.030	S5(96)	ν_{as} C(4)−H
ν_2	3005 vw	3011	0.045	S6(98)	A ν_{AS} C−H	3020	0.025	S6(96)	ν_{as} C(4)−H
	3005 vw	3011	0.086	S23(98)	B ν_{as} C−H	3013	0.416	S23(100)	ν_{as} C(10)−H
ν_3	2952 vw	2928	0.025	S4(97)	A ν_s C−H	2931	0.316	S21(89)	ν_s C(4)−H
	2952 vw	2928	0.017	S21(97)	B ν_s C−H	2930	0.060	S4(89)	ν_s C(10)−H
ν_4	1835 s	1845	5.659	S2(81)	A ν C═O	1834	4.046	S2(86)	ν C2═O3
ν_5	1779 s	1777	1.702	S19(88)	B ν C═O	1776	4.158	S19(83)	ν C8═O9
ν_6	1435 w	1444	0.043	S8(84)	A δ_{as} C−H	1450	0.361	S8(47),S9(41)	δ_{as} C(4)−H
	1435 w	1443	0.319	S25(84)	B δ_{as} C−H	1444	5.439	S25(83)	δ_{as} C(10)−H
		1441	0.533	S9(84)	A δ_{as} C−H	1441	0.658	S26(81)	δ_{as} C(10)−H
		1440	0.143	S23(86)	B δ_{as} C−H	1437	0.273	S9(47),S8(41)	δ_{as} C(4)−H
ν_7	1375 m	1368	0.221	S7(86)	A δ_s C−H	1370	4.055	S24(85)	δ_s C(10)−H
	1375 m	1363	1.753	S21(92)	B δ_s C−H	1360	1.232	S7(89)	δ_s C(4)−H
ν_8	1230 m	1224	0.094	S3(26),S1(16), S13(20)	A ν C−C A ν C−O	1247	3.287	S18(23),S20(18)	ν C(8)−O(1) ν C(8)−C(10)
ν_9	1135 vs	1141	14.767	S27(30),S3(22), S1(15)	B ν C−O, ν C−C	1134	9.007	S10(30),S3(19)	ρ C(4)−H ν C(2)−C(4)
ν_{10}	1070 w	1052	0.054	S11(62),S14(22)	A ρ C−H	1059	0.141	S11(58),S14(23)	ρ C(4)−H
	1070 w	1041	0.305	S28(65),S31(22)	B ρ C−H	1046	0.799	S28(66),S31(23)	ρ C(10)−H
ν_{11}	1002 s	1009	0.048	S10(51),S3(15)	A ρ C−H	1004	2.854	S27(54),S29(10)	ρ C(10)−H
	1002 s	988	7.063	S27(44),S18(15)	B ρ C−H B ν C−O	985	0.834	S10(40),S3(28)	ρ C(4)−H ν C(2)−C(4)
ν_{12}	900 m	889	2.525	S18(56),S19(36)	B ν C−C B ν C═O	901	3.068	S18(42),S20(27)	ν C(8)−O(1) ν C(8)−C(10)
ν_{13}	785 m	796	0.414	S1(52),S12(12)	A ν C−O A δ O−C−C	778	1.306	S1(36),S3(17)	ν C(2)−O(1) ν C(2)−C(4)
ν_{14}	655 vw	670	0.002	S3(38),S13(38)	A ν C−C A ρ O═C−C	647	0.062	S30(20),S14(15),S20(14)	ν C(8)−C(1) π C(2)═O(3) δ O(3)═C(2)−C(4) δ O(9)═C(8)−C(10)
ν_{15}	598 w	587	0.511	S31(70),S27(20)	B π O═C−C B ρ C−H	599	0.173	S31(44),S28(14)	π C(8)═O(9) δ O(3)═C(2)−C(4) ρ C(10)−H
ν_{16}	554 w	554	0.004	S14(70),S10(18)	A π O═C−C A ρ C−H	556	1.028	S13(38),S31(22)	π C(8)═O(9) δ O(3)═C(2)−C(4)
ν_{17}	534 w	520	0.412	S30(74)	B δ O═C−C	526	0.009	S14(48),S13(12)	π C(2)═O(3) ρ O(3)═C(2)−C(4)
ν_{18}	430 w	407	0.012	S29(86)	B δ O═C−C	424	0.075	S12(58),S30(14)	δ O(3)═C(2)−C(4) ρ O(9)═C(8)−C(10)
ν_{19}	310 w	334	0.028	S12(43),S21(14)	A δ O═C−C	341	0.016	S29(40),S12(18)	δ O(9)═C(8)−C(10) δ O(3)═C(2)−C(4)
ν_{20}	192 w	194	0.021	S17(73),S12(22)	A δ C−O−C	193	0.112	S17(64),S29(15)	δ C(2)−O(1)-C(8)
ν_{21}	130 w	124	0.000	S15(55),S16(43)	A ι C−H	132	0.004	S15(95)	ι C(4)−H
ν_{22}	106 w	123	0.004	S33(75),S32(47)	B ι C−H	107	0.069	S33(51),S32(49)	ι C(10)−H ιC(8)−O(1)
ν_{23}	80 w	71	0.036	S33(50),S32(49)	B ι C−O	79	1.220	S33(48),S32(45)	ι C(8)−O(1) ι C(10)−H
		51	0.037	S33(50),S16(43)	A ι C−O	35	0.110	S16(97)	ι C(2)−O(1) δ C−O−C

[a] ν, stretching; δ, bending; ρ, rocking; π, out-of-plane bending; ι, torsion; w, weak; s, strong; m, moderate; vs, very strong; unit of frequency, cm^{-1}; calculated intensity, 10^6cm/mol. [b] Contributions less than 10% to potential energy distribution are omitted.

model, together with the calculated intensities (Table 5), yields a calculated ratio $I(\upsilon_5)/I(\upsilon_4)$ in the interval 0.60−0.86. This is in agreement with the ratio $I(\upsilon_5)/I(\upsilon_4) = 0.80(3)$ we obtained by triangulation of the experimental C═O bands in the gas phase. The model also rationalizes the spectral changes that can be seen when AA goes from the gaseous state via various solutions, including the pure liquid, to the crystalline state. In this sequence, the intensity of the υ_4 band increases and that of the υ_5 band decreases (see Figure 5). This suggests an increasing amount of the nonplanar (sp,sp) form. The crystal structure of monochloroacetic anhydride, in which only a quasi-C_2 form is present,[29] supports this. Moreover, it rationalizes the observation of a growing contribution of the highly polar (sp,sp) form (calculated dipole moment = 4.2 D) with solvent polarity and concomitant decrease of the ratio $I(\upsilon_5)/I(\upsilon_4)$.

1600−350 cm^{-1} Region. This spectral region is complicated as well as intriguing. It is complicated, because in it are collected all C−O and C−C stretchings and various bending modes, most of which are strongly mixed. It is intriguing, because it contains a doublet near 800 cm^{-1}, the behavior of which in different aggregation phases remained unexplained so far.

Of the 14 bands observed in this region, those at 1435 cm^{-1} (υ_6) and at 1375 cm^{-1} (υ_7) are well localized and are assigned to the antisymmetric and symmetric CH_3 bending modes, respectively. The other bands, υ_8 through υ_{19}, show low percentages of localized vibrations and may therefore be classified as skeletal vibrations. This attitude was taken by Mirone et al.[4] The largest localized part (Table 3), however, agrees in general with the normal coordinate analysis results of Vledder et al.,[5] thereby reconciling most of the discrepancies in previous assignments.

The model will now be used to predict and explain phase-dependent features of bands in this region from the comparison of gas-phase spectra with those of a 0.2 M solution in CCl_4.

TABLE 6: Models Which Were Refined Simultaneously, with the Parameters of Pseudoconformers Taken from ab Initio (MP2/6-31G)**

	[sp,sp] O(9)═C(8)−O(1)−C(2)/ O(3)═C(2)−O(1)−C(8)					[sp,ac] O(9)═C(8)−O(1)−C(2)/ O(3)═C(2)−O(1)−C(8)		
parameters[a]	20/20	20/40	20/60	20/80	40/40	0/100	0/120	0/140
O(1)−C(2)	1.402	1.396	1.387	1.378	1.401	1.372	1.375	1.379
O(1)−C(8)	1.402	1.407	1.417	1.429	1.401	1.433	1.427	1.418
C(2)═O(3)	1.207	1.208	1.211	1.215	1.208	1.217	1.216	1.214
C(8)═O(9)	1.207	1.206	1.205	1.203	1.208	1.203	1.204	1.206
C(2)−C(4)	1.502	1.501	1.500	1.500	1.498	1.501	1.501	1.501
C(8)−C(10)	1.502	1.499	1.496	1.494	1.498	1.496	1.498	1.500
C(8)O(1)C(2)	120.5	118.5	116.2	114.2	117.0	114.6	118.2	121.4
O(1)C(2)O(3)	124.5	123.7	122.9	122.6	122.3	122.9	123.9	124.6
O(1)C(8)C(9)	124.5	123.0	121.5	120.2	122.3	119.7	118.4	117.1
O(1)C(2)C(4)	108.5	109.2	110.0	110.5	110.2	110.4	109.8	109.1
O(1)C(3)C(7)	108.5	109.6	110.6	110.5	110.2	112.2	114.1	116.8
m,[b] %	6.4	19.9	14.0	8.3	8.2	13.7	16.4	13.1

[a] Bond lengths in angstroms, angles in degrees. [b] Weight of conformers.

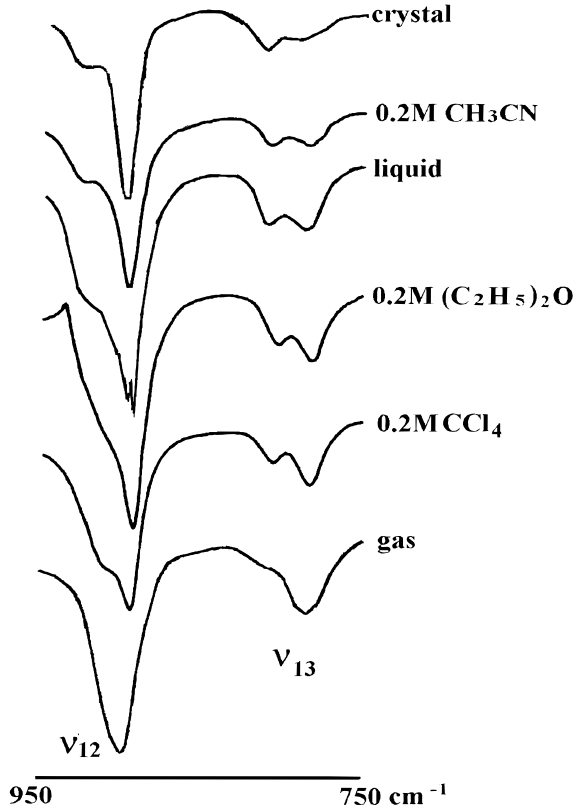

Figure 7. Phase dependency of the bands υ_{12} and υ_{13}.

Going from the gas phase to the CCl_4 solution, the observed intensity ratio $I(\upsilon_5)/I(\upsilon_4)$ changes from 0.80 to 0.65, from which we calculate that the ratio nonplanar (sp,sp)/(sp,ac) changes from 25%:75% to 40%:60%. The nonpolar CCl_4 ($\epsilon = 2.2$) induces only a small change in the rotamer composition (i.e., range of the large-amplitude motion), but its small reaction field should allow use of the calculated gas-phase IR frequencies and intensities also for the solution spectra. It can be deduced that the experimental and theoretical uncertainties, in particular the inherently low resolution of the AA bands, limit us to examining only bands of medium and higher intensity, of which the calculated frequencies of the nonplanar (sp,sp) and (sp,ac) forms differ by more than 10 cm^{-1} and/or their calculated intensities by more than 10%.

Bands υ_8, υ_{12}, and υ_{13} meet the criteria and are indeed the only ones to show phase-dependent IR behavior (see Figures 6 and 7); so far, only that of υ_{13} had been noted before.[4,5]

TABLE 7: Dynamic Models for "the Conformers" with Refinable Parameters and Constraints

parameter[a]	nonplanar [sp,sp]	[sp,ap]
O(1)−C(2)	r1	r2
O(1)−C(8)	r1	r3
C(2)═O(3)	r4	r4
C(8)═O(9)	r4	r4 + Δ[b]
⟨C−C⟩	r5	r5
⟨C−H⟩	r6	r6
C(2)−O(1)−C(8)	θ7	θ8
O(1)−C(2)═O(3)	θ9	θ10
O(1)−C(2)-C(4)	θ11	θ12
O(1)−C(8)═O(9)	θ9	θ13
O(1)−C(8)−C(10)	θ11	θ14
⟨C−C−H⟩[c]	fixed	fixed
O(9)═C(8)−O(1)−C(2)	φ15	φ16
O(3)═C(2)−O(1)−C(8)	φ15	φ17

[a] For the numbering scheme see Figure 1. [b] $\Delta = 0.012$ (average value from ab initio). [c] 104°.

Recalling that the model predicts an increase in the nonplanar (sp,sp) form with increasing polarity, it follows that the low-frequency component of the doublet (υ_{13}) near 800 cm^{-1} (Figure 7) belongs to the (sp,ac) form, being predominantly present in the gas phase. The high-frequency component, clearly visible in polar solutions and in the crystal, is attributed to the nonplanar (sp,sp) form. Furthermore, the gas-phase intensity of the low-frequency component being calculated as 5 times higher than that of the high-frequency component agrees with the observation. The composition of liquid AA ($\epsilon = 22$), as estimated from the intensity ratio, is 73% nonplanar (sp,sp) to 27% (sp,ac). Similarly, the low-frequency component of υ_{12}, observed as increasing in intensity with polarity, can be assigned to the nonplanar (sp,sp) form, and the high-frequency shoulder to the (sp,ac). The latter completely merges with the former, losing all resolution, in the gas phase.

Finally, υ_8, also devoid of resolution, is predicted to and indeed shows (Figure 6) a significant decrease in intensity on going from the gas phase to the CCl_4 solution, thereby only decreasing the strongly absorbing (sp,ac) form by 10%.

Region below 350 cm^{-1}. The region contains five weak bands, none of which has been reported before. They are assigned, as shown in Table 5, to O═C−C and C−O−C rocking and bending motions, and to C−O and C−H torsions. Despite the fact that the harmonic approximation becomes less suitable for motions with small force constants, the root-mean-square deviation between calculated and observed frequencies in this region is still only 12 cm^{-1}, and all calculated intensities are weak, in agreement with the observations.

TABLE 8: Selected Root-Mean-Square Vibrational Amplitudes, U_{ij}, and Perpendicular Amplitudes, K_{ij}, Calculated from the MP2/6-31G Force Field**

	[sp,sp]			[sp,ac]		
atom pair	U_{ij}(calc)	U_{ij}(ED)	K_{ij}	U_{ij}(calc)	U_{ij}(ED)	K_{ij}
O(1)−C(2)	0.051	fixed	0.0018	0.050	fixed	0.0018
O(1)−C(8)	0.051		0.0018	0.049		0.0017
C(2)═O(3)	0.037		0.0011	0.037		0.0011
C(8)═O(9)	0.037		0.0011	0.037		0.0011
C(2)−C(4)	0.050		0.0016	0.050		0.0016
C(8)−C(10)	0.050		0.0016	0.050		0.0016
⟨C−H⟩	0.077		0.0054	0.076		0.0053
O(1)···O(3)	0.055		0.0044	0.056		0.0045
O(1)···C(4)	0.067		0.0056	0.064		0.0054
O(1)···O(9)	0.055		0.0043	0.056		0.0045
O(1)···C(10)	0.066		0.0056	0.068		0.0055
O(9)···C(10)	0.060		0.0049	0.060		0.0048
O(3)···C(4)	0.059		0.0049	0.060		0.0048
C(2)···C(8)	0.063		0.0033	0.065		0.0035
O(3)···O(9)[a]	0.134	0.169(25)	0.0074	0.078	0.142(24)	0.0059
O(3)···C(10)[a]	0.079	0.067(23)	0.0084	0.131	0.240(25)	0.0089
C(4)···C(8)[a]	0.069	0.162(24)	0.0076	0.070	0.182(24)	0.0081
C(4)···O(9)[a]	0.080	0.169(23)	0.0087	0.071	0.084(23)	0.0101
C(4)···C(10)[a]	0.088	0.094(75)	0.0124	0.080	0.089(23)	0.0112
C(2)···O(9)[a]	0.090	0.175(25)	0.0053	0.061	0.090(31)	0.0057
O(3)···C(8)[a]	0.090	0.126(25)	0.0053	0.094	0.094(25)	0.0052
C(2)···C(10)[a]	0.069	0.146(23)	0.0077	0.087	0.160(68)	0.0069

[a] Bond distances dependent from dihedral angles.

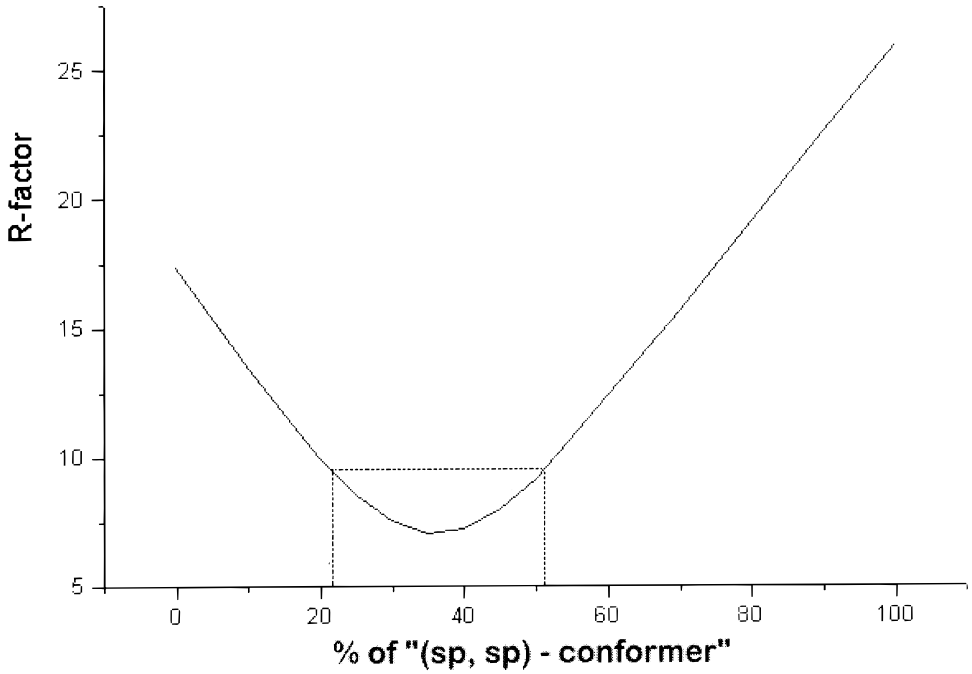

Figure 8. Disagreement factor *R* between the experimental electron diffraction *sM*(s) values and those of the dynamic model consisting of eight pseudoconformers in function of the percentage of the so-called "nonplanar (sp,sp) conformer" (see text); error bars are shown for 99% level of significance.

Electron Diffraction

The theory describing the effects a multiple rotor exerts on electron diffraction intensities is explored in a number of seminal papers and texts by Karle, Hedberg, Lowrey, Mijlhoff, and others.[30−36] Following their approach, the AA molecule shows large-amplitude motions. Hence, the molecule was described by using all pseudoconformers at 20° intervals on the relevant part of the rotation.[36] For the calculations Hartree−Fock and Moller−Plesset approximations were used.

We tested more than 300 conformers on the rotation paths and calculated their energy on the HF/4-21G level. Of these, 22 models were selected which have an energy less than 3 kcal/mol above the nearest energy minimum (i.e., the nonplanar (sp,sp) and (sp,ac) form). The geometrical parameters of these 22 pseudoconformers were then optimized on the MP2/6-31G** level. Next, a further approximation was introduced; only those pseudoconformers were retained that contribute at least 5% to the total conformers population. This reduced the number of pseudoconformers to eight, five of which cluster around the nonplanar (sp,sp) energy minimum and may be collectively named "the nonplanar (sp,sp) conformer", and three cluster around the (sp,ac) minimum and may be collectively called "the (sp,ac) conformer". Finally, weights were calculated assuming a Boltzmann distribution of contributing species in the two-

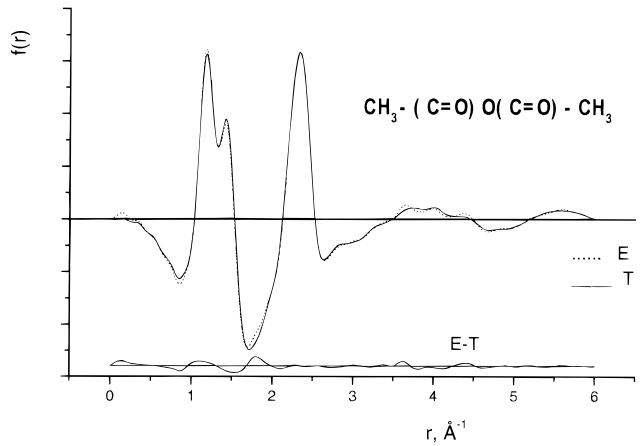

Figure 9. Comparison of the theoretical radial distribution function (solid line) with the experimental one (dots). The difference between the theoretical and experimental curves is given as E−T; a damping factor of 0.002 was used and no $sM(s)$ values below $s = 4.0$ Å^{-1} were used.

dimensional torsion space. It should be noted that for AA, forms of C_1 symmetry have multiplicity number $g(C_1) = 4$ and those of C_2 symmetry have $g(C_2) = 2$. The normalized weights (m in %) are listed in Table 6, together with the geometrical parameters of the heavy-atom skeletons.

In the initial stage of the structural analysis, we assumed C_1 symmetry for the (sp,sp)-like pseudoconformers. However, after minimization, the values of ϕ_1 (O(9)═C(8)−O(1)−C(2)) and ϕ_2 (O(3)═C(2)−O(1)−C(8)) turned out to be close to each other. Hence, in the further analysis C_2 symmetry was accepted for them. Furthermore, the geometry calculations justify to consider all C−H and C−C distances, as well as all C−C−H valence angles independent of the ϕ_1 and ϕ_2 values. Moreover, in all pseudoconformers it is justified to use local C_{3v} symmetry in the CH_3 groups and local C_s symmetry in the C−C(O)−O moieties. However, it is often assumed that the torsion angle parameters (ϕ_1, ϕ_2) themselves are the *only* torsion-dependent geometrical parameters and that *one* harmonic force field suffices to calculate all u_{ij} and K_{ij} values. The differences in skeletal bond lengths and valence angles (Table 6) and even in IR frequencies (Table 5) between the nonplanar (sp,sp) and (sp,ac) (pseudo)conformers show that this assumption is not correct for AA. Hence, it seems worthwhile to discuss in some detail the construction of the remaining part of the dynamic model to be used in the least-squares analyses. Apart from the two torsion angles, we used 15 geometrical parameters (see Table 7). The choice was made upon an inspection of Table 2, which shows that, e.g., the differences between the various CO lengths strongly depend on the method of calculation (DFT or MP2). Similar discrepancies exist in other parameters. Therefore, we introduced the main geometrical parameters for the two "conformers" separately as independent parameters, while the geometrical parameters of the pseudoconformers were constrained to those of their corresponding "conformers" using the MP2/6-31G** data shown in Tables 2 and 6.

In the next step, the effect of the internal rotations on the vibrational amplitudes, u_{ij}, and the K_{ij} corrections had to be eliminated, remembering that the dynamic model describes the molecule as a mixture of eight pseudoconformers. For this the (MP2/6-31G** calculated) force constants corresponding to internal rotations in the two "conformers" were set to infinity. Using the initial (MP2/6-31G** calculated) values of the geometrical parameters and force fields, 76 vibrational u_{ij} and K_{ij} values for each pseudoconformer were obtained. Since there are eight pseudoconformers, the initial model contained 608 u_{ij} and K_{ij} values. A selection of these for the two main "conformers" is presented in Table 8. Vibrational amplitudes (u_{ij}) and perpendicular corrections (K_{ij}) were also calculated for the frame of the eight pseudoconformers and for the rotational parts of the AA molecule.

In the subsequent least-squares analysis of the electron diffraction data, we kept the vibrational parameters fixed for the framework distances and refined those belonging to the interatomic distances which depend on the torsion angles ϕ_1 and ϕ_2. At this point, we want to mention that the actual calculations of u_{ij} and K_{ij} values connecting the ab initio r_e -type distances to electron diffraction r_a distances were performed with a program devised by Sipachev.[37] The program calculates the mean square vibrational amplitudes of interatomic distance variations and the corrections for the Bastiansen−Morino shrinkage effect extending the theory described by Cyvin.[38] Unlike the standard procedure to convert an r_α-structure (close to r_e) to an r_a-structure, the algorithm used in this work takes into account not only the squares of the perpendicular amplitudes but also other second-order terms with respect to atomic displacements from the equilibrium positions that appear in solving the vibrational problem in the harmonic approximation. Note that in agreement with physical intuition and unlike the conventional calculation procedure,[38] calculations by the scheme suggested in ref 37 give zero or negligibly small corrections for bonded and short nonbonded distances and large corrections for long interatomic distances depending on a number of vibrational coordinates and therefore more liable to distortions resulting from vibrational effects.

Ultimately, we refined 17 geometrical parameters and five groups of vibrational amplitudes. In the final stage of the structural analysis using a step-by-step optimization (see Figure 8) we found that the proportion of the sum of pseudoconformers close to (sp,sp) [i.e., the nonplanar (sp,sp) "conformer"] to the sum of pseudoconformers close to (sp,ac) [i.e., the (sp,ac) "conformer"] is 37 ± 15% and 63 ± 15% on a 99% significance level.[26] The final radial distribution function is shown in Figure 9. The resulting optimized parameters and the correlation coefficients between them are listed in Tables 9 and 10, respectively.

Although the error limits are large, the experimental "conformer" ratio translates into an energy difference E(sp,ac) − E(sp,sp) = 0.1 kcal/mol, which compares gratifyingly well with the theoretical ones (Table 1), except for HF/4-21G.

A comparison of the geometrical parameters of AA with those of similar molecules, shown in Table 9, reveals the following. First, the C(2)−O(1)−C(8) angles are practically equal to those in formic anhydride HC(O)OC(O)H[2] and in formic acetic anhydride HC(O)OC(O)CH_3[3]. The latter angle in the "nonplanar (sp,sp) conformer" of AA (116.5°) fits into the normal increase of the COC angle from 112° via 116° to 118°, seen[38] to occur when C(sp^3) is progressively replaced by C(sp^2). The further increase to 121° in the (sp,ac) "conformer" of AA reflects the strong repulsive interactions (dipole−dipole repulsion and steric hindrance) that exist between the acetyl moieties of AA. Second, in AA as well as in formic anhydride (FA) and the mixed formic acetic anhydride (FAA) shorter C═O and longer C−O bonds are found[2,3] than in the corresponding carboxylic acids and esters.[39] These observations point to a weaker resonance in the O═C−O−C═O moiety of anhydrides compared to the O═C−O−R moiety of esters which helps to rationalize why anhydrides are more reactive toward nucleophilic agents than esters. Third, AA is a floppy molecule, however, with good thermal stability,

TABLE 9: Best[a] Fitting Geometry of Acetic Anhydride Conformers and Related Molecules in Angstroms and Degrees from ED and ab Initio (MP2/6-31G)**

	acetic anhydride					
	sp,sp[b]		sp,ac[c]		FA (ED)	FAA (ED)
parameters	r_g, $\angle_\alpha$ (ED)	r_e, $\angle_e$ (AI)	r_g, $\angle_\alpha$ (ED)	r_e, $\angle_e$ (AI)	r_g, $\angle_\alpha$[2]	r_g, $\angle_\alpha$[3]
O(1)−C(2)	1.370(15)[d]	1.400	1.406(6)	1.430	1.397(8)	1.380(8)
O(1)−C(8)	1.370(15)	1.400	1.370(13)	1.369	1.378(8)	1.380(8)
C(2)═O(3)	1.182(3)	1.200	1.182(3)	1.195	1.189(8)	1.187(8)
C(8)═O(9)	1.182(3)	1.200	1.194(3)	1.210	1.196(8)	1.195(8)
⟨C−C⟩	1.489(2)	1.501	1.489(2)	1.501		1.500(8)
⟨C−H⟩	1.099(4)	1.094	1.099(4)	1.094	1.105(15)	1.082(15)
C(2)−O(1)−C(8)	116.5(20)	118.6	121.0(15)	115.9	118.6(5)	119.8(5)
O(1)−C(2)═O(3)	124.8(20)	123.7	124.2(18)	118.8	124.2(5)	122.4(5)
O(1)−C(2)−C(4)	114.6(23)	109.0	111.1(22)	113.2		110.2(5)
O(1)−C(8)═O(9)	124.8(20)	123.7	117.1(10)	123.5	120.8(5)	121.7(5)
O(1)−C(8)−C(10)	114.6(23)	109.0	110.9(17)	110.1		
O(9)═C(8)−O(1)−C(2)	30.9(67)	26.9	−27.4(53)	−2.3	0	0
O(3)═C(2)−O(1)−C(8)	30.9(67)	26.9	122.0(39)	113.2	180	180

[a] *R*-factor for dynamic models is 6.87%. [b] Sum models with torsion angles O(9)═C(8)−O(1)−C(2)/O(3)═C(2)−O(1)-C(8): 20/20, 20/40, 20/60, 20/80, 40/40 (see Table 6). [c] Sum models: 0/100, 0/120, 0/140 (see Table 6). [d] Values in parentheses are estimated standard deviations from least squares.

TABLE 10: Correlation Coefficients (×100) among Parameters[a]

	r1	r2	r3	r4	r5	r6	θ_7	θ_8	θ_9	θ_{10}	θ_{11}	θ_{12}	θ_{13}	θ_{14}	φ_{15}	φ_{16}	φ_{17}	$k(u)$
r1	100																	
r2	−87	100																
r3	−14	−29	100															
r4	7	20	−52	100														
r5	4	26	−59	37	100													
r6	21	−19	12	−7	−23	100												
θ_7	−7	25	−25	36	−36	7	100											
θ_8	6	−9	0	−6	−8	1	−47	100										
θ_9	−75	56	22	−31	−20	−31	−48	21	100									
θ_{10}	−29	43	−22	20	28	10	70	−49	−28	100								
θ_{11}	−24	17	7	−6	−9	−1	37	−66	−3	44	100							
θ_{12}	−66	45	22	−35	−38	−14	−40	−12	79	2	44	100						
θ_{13}	89	−94	22	−10	−16	35	−5	89	−73	−23	11	−56	100					
θ_{14}	47	−42	−6	7	2	12	27	−63	−53	9	20	−29	48	100				
φ_{15}	−18	15	15	−15	−19	12	−39	54	27	−21	−31	−15	−54	−54	100			
φ_{16}	−69	0	0	−4	3	−5	10	−8	43	47	39	52	−47	−47	38	100		
φ_{17}	68	5	5	−2	−11	11	−18	9	−45	−43	−36	−44	67	65	17	−67	100	
$k(u)$	−19	18	−29	12	35	−70	8	−3	21	1	6	3	−32	−7	−18	4	−11	100

[a] See Table 7 for definition of parameters.

whereas FA and FAA are rigid, planar molecules with little thermal stability.[2,3]

Conclusions

It emerges from the ab initio calculations that AA exhibits skeletal motions with large amplitudes. Inspection of Figure 1 shows that for the planar forms the steric hindrance increases on going from [sp,sp] → [sp,ap] → [ap,ap], while the dipole−dipole repulsion increases on going in the opposite direction. The destabilizing interactions are relieved in the nonplanar forms, although at the expense of some mesomeric stabilization. Hence, the delicate balance of these interactions allows in AA for a wide variation in skeletal torsion and valence angles to occur without much variation in internal energy. The different geometries along the rotation paths can be rationalized in terms of mesomeric and steric effects. One meets along the rotation pathways an equilibrium between three (sp,ac) forms (collectively called "(sp,ac) conformer") and five nonplanar (sp,sp) forms (collectively called "nonplanar (sp,sp) conformer") with multiplicity numbers 4 and 2, respectively. Scaled MP2/6-31G** force fields of these two "conformers" were used to analyze the electron diffraction intensities in the gas phase as well as the IR frequencies and intensities of AA in the gas phase and in solutions. In the least-squares analysis of the electron diffraction data, a dynamic model was employed in which an "(sp,ac) conformer" was represented by three pseudoconformers with semifixed ϕ_1 and ϕ_2 values, but relaxed geometry otherwise, and a "nonplanar (sp,sp) conformer" was represented in a similar way by five pseudoconformers. This model translated into an experimental energy difference E(sp,ac) − E(sp,sp) = 0.1 kcal/mol, in line with the large-amplitude model as well as with sophisticated quantum chemical results. Furthermore, the model reproduced the gas-phase IR frequencies with root-mean-square deviations of about 10 cm^{-1} and resulted in an improved frequency assignment.

Moreover, it explains much discussed peculiarities of the spectra, in particular (i) the occurrence of many weak bands and (ii) the changes in band intensities (υ_4, υ_5, υ_8), band shape (υ_{12}) and doublet behavior (υ_{13}) when going from the gas phase to the liquid phase and to the solutions in solvents of different polarities. Thereby, the model is self-consistent, removing apparent discrepancies and unifying results of previous and present IR and ED experiments.

Acknowledgment. We thank Prof. Dr. L. V. Vilkov (Moscow) for valuable remarks made during the preparation of this manuscript. C.V.A. thanks the Flemish Science Foundation (FWO) for an appointment as "onderzoeksdirecteur", I.F.Sh.

thanks the Special Research Fund of Antwerp University for a postdoctoral fellowship, and I.F.Sh. and L.K. are grateful to the Russian RFBR (Project N 96-03000008G). Financial support to the UIA laboratory by the University of Antwerpen under Grant GOA-BOF-UA No. 23 is gratefully acknowledged.

Supporting Information Available: Electron diffraction intensities, $I(s)$, and leveled intensities, $sM(s)$, of AA are available. This material is available free of charge via the Internet at http://pubs.acs.org.

References and Notes

(1) *IUPAC 1974, Rules for the Nomenclature of Organic Chemistry, Section E: Stereochemistry, Recommendations*; Pergamon Press: Oxford, 1974.

(2) Wu, G.; Shlykov, S.; Van Alsenoy, C.; Geise, H. J.; Sluyts, E.; Van der Veken, B. J. *J. Phys. Chem.* **1995**, *99*, 8589.

(3) Wu, G.; Shlykov, S.; Van Alsenoy, C.; Geise, H. J.; Sluyts, E.; Van der Veken, B. J. *J. Phys. Chem.* **1996**, *100*, 11620.

(4) Mirone, P.; Fortunato, B.; Canziani, P. *J. Mol. Struct.* **1970**, *5*, 283.

(5) Vledder, H. J.; Van Kleef, F. S. M.; Mijlhoff, F. C.; Leyte, J. C. *J. Mol. Struct.* **1971**, *10*, 189.

(6) Vledder, H. J.; Mijlhoff, F. C.; Leyte, J. C.; Romers, C. *J. Mol. Struct.* **1971**, *7*, 421.

(7) Colthup, N. B. *Appl. Spectrosc.* **1985**, *6*, 1030.

(8) Shlykov, S. A.; Tremmel, J.; Van Loock, J.; Geise, H. J. *J. Mol. Struct.* **1997**, *413*−*414*, 579.

(9) Tamagawa, K.; Iijima, T.; Kimura, M. *J. Mol. Struct.* **1976**, *30*, 243.

(10) Van Loock, J. F.; Van den Enden, L.; Geise, H. J. *J. Phys. E* **1983**, *16*, 255.

(11) Forster, H. R. *J. Appl. Phys.* **1970**, *41*, 5344.

(12) Ross, A. W.; Fink, M.; Hilderbrandt, R. In *International Tables of X-ray Crystallography*; Wilson, A. J. C., Ed.; Kluwer Academic Publishers: Dordrecht, The Netherlands, 1992; Vol. C, p 245.

(13) Tavard, C.; Nicolas, D.; Rouault, M. *J. Chim. Phys. Chim. Biol.* **1964**, *40*, 1686.

(14) Van den Enden, L.; Van Laere, E.; Geise, H. J.; Mijlhoff, F. C.; Spelbos, A. *Bull. Soc. Chim. Belg.* **1976**, *85*, 735.

(15) Tremmel, J.; Hargittai, I. In *Stereochemical Application of Gas-Phase Electron Diffraction*; Hargittai, I., Hargittai, M., Eds.; VCH Publishers: Deerfield Beach, FL, 1988; Part A, Chapter 6.

(16) Vilkov, L. V.; Mastryukov, V. S.; Sadova, N. I. *Determination of the Geometrical Structure of Free Molecules*; Mir Publishers: Moscow, 1983; Chapter 1.

(17) Pulay, P. *Mol. Phys.* **1969**, *17*, 97.

(18) Pulay, P. *Theor. Chim. Acta*, **1979**, *50*, 299.

(19) Pulay, P. In *Modern Theoretical Chemistry*; Schäfer, H. F., III, Ed.; Plenum Press: New York, 1977; Vol. 4, pp 154ff.

(20) Van Alsenoy, C.; Peeters, A. *J. Mol. Struct. (THEOCHEM)* **1993**, *286*, 18.

(21) Frisch, M. J.; Trucks, G. W.; Schlegel, H. B.; Gill, P. M. W.; Johnson, B. G.; Robb, M. A.; Cheeseman, J. R.; Keith, T. A.; Petersson, G. A.; Montgomery, J. A.; Raghavachari, K.; Al-lahama, M. A.; Zakrzewski, V. G.; Ortiz, J. V.; Foresman, J. B.; Cioslowski, J.; Stefanov, B. B.; Nanayakkara, A.; Challacombe, M.; Peng, C. Y.; Ayala, P. Y.; Chen, W.; Wong, M. W.; Andres, J. L.; Replogle, E. S.; Gomperts, R.; Martin, R. L.; Fox, D. J.; Binkley, S.; Defrees, D. J.; Baker, J.; Stewart, J. P.; Head-Gordon, M.; Gonzalez, C.; Pople, J. A. *Gaussian 94*, revision D; Gaussian Inc.: Pittsburgh, PA, 1995.

(22) Bunker, P. R. In *Molecular Symmetry and Spectroscopy*; Academic Press: New York, 1979; Chapters 1 and 2.

(23) Krasnoshchiokov, S. V.; Abramenkov, A. V.; Panchenko, N. Y. *Zh. Fiz. Khim.* **1997**, *71*, 497 (in Russian).

(24) Forsythe, G. E.; Malcolm, M. A.; Moler, C. B. In *Computer methods for mathematical computations*; Prentice Hall: New York, 1977.

(25) Pulay, P.; Fogarasi, G.; Pang, F.; Boggs, J. E. *J. Am. Chem. Soc.* **1979**, *101*, 2550.

(26) Hamilton, W. C. *Statistics in Physical Sience*; Ronald Press: New York, 1964; pp 157 ff.

(27) Mirone, P.; Chiorboli, P. *Rend. Accad. Nazl. Lincei* **1961**, *30* (8), 214.

(28) Fayat, C.; Foucaud, A.; *C. R. Acad. Sci. Paris* **1967**, *265*, 345.

(29) De Kok, A. J.; Romers, C. *Recl. Trav. Chem. Pays-Bas* **1969**, *88*, 625.

(30) Karle, J. *J. Chem. Phys.* **1973**, *59*, 3659.

(31) Karle, J. In *Diffraction Studies on Non-Crystalline Substances*; Hargittai, I., Orville-Thomas, W. J., Eds.; Elsevier: Amsterdam, 1981; pp 243 ff.

(32) Orville-Thomas, W. J., Ed.; *Internal Rotation in Molecules*; John Wiley: London, 1974.

(33) Lister, D. G.; Macdonald, J. N.; Owen, N. L. *Internal Rotation and Inversion*; Academic Press: New York, 1978.

(34) Danielsen, J.; Hedberg, K. *J. Am. Chem. Soc.* **1979**, *101*, 3199.

(35) Lowrey, A. H. In *Diffraction Studies on Non-Crystalline Substances*; Hargittai, I.; Orville-Thomas, W. J., Eds.; Elsevier: Amsterdam, 1981; pp 197 ff.

(36) Ter Brake, J. H. M.; Mijlhoff, F. C. *J. Mol Struct.* **1981**, *77*, 109.

(37) Sipachev, V. A. *J. Mol. Struct. (THEOCHEM)* **1985**, *121*, 143.

(38) Cyvin, S. J. *Molecular Vibrations and Mean Square Amplitudes*; Universitets forlaget: Oslo, 1968.

(39) Naumov V. A. In *Stereochemical Application of Gas-Phase Electron Diffraction*; Hargittai, I., Hargittai, M., Eds.; VCH: Deerfield Beach, FL, 1988; Part B, Chapter 3.